Journal of Catalysis **210,** 263–272 (2002)
doi:10.1006/jcat.2002.3687

Hydrogen Production Using Ni–Rh on ZrO_2 as Potential Low-Temperature Catalysts for Membrane Reactors

S. Irusta, L. M. Cornaglia, and E. A. Lombardo[1]

Instituto de Investigaciones en Catálisis y Petroquímica (FIQ, UNL-CONICET), Santiago del Estero, 2829-3000 Santa Fe, Argentina

Received November 7, 2001; revised May 9, 2002; accepted May 30, 2002

The CO_2 reforming of CH_4 over Ni–Rh mono- and bimetallic catalysts supported on ZrO_2 was investigated. The catalysts were prepared by wet impregnation with 0.2 wt% Rh and 2 wt% Ni. The solids were calcined at 823 K in air flow and were reduced at 973 K in flowing hydrogen before being tested in a fixed-bed reactor. The results showed that the bimetallic solid had the highest activity at 823 K but monometallic Rh was the only stable catalyst. The catalysts were characterized through XRD, XPS, and TPR. TGA, DSC, TPH, SEM, and Raman spectroscopy were used in order to characterize the carbonaceous deposits. Carbon deposits with different reactivity were detected. A low-carbon deposition was observed on Rh (0.2%)/ZrO_2which exhibited a stable activity after 100 h on stream. The results suggest a significant metal–support interaction and a strong metal–metal interaction in the bimetallic solid.

Key Words: **hydrogen; CO_2 reforming; Ni–Rh catalysts.**

INTRODUCTION

The dry reforming of methane is an attractive route to produce H_2 from natural gas. This is even more appealing if a membrane reactor can be used to produce high-purity H_2 (1).

The two most wanted features of the candidate catalysts for this process are low-carbon formation and good stability at low reaction temperatures. Both the metal and the support used are key players in the development of these features. Wang and Ruckenstein (2) found that both the activity and stability of Rh formulations are strongly dependent on the support. On the other hand, Bitter *et al.* (3) stated that the activity of Rh-containing catalysts is only a function of the metal exposed and is not affected by the support. Ni has been supported over different solids (4). In all cases, the support plays a key role in coke deactivation and metal sintering (5). Montoya *et al.* (6) studied the catalytic behavior of Ni supported on Ce-modified ZrO_2. It showed good activity but the amount of carbonaceous deposits was higher in Ni/ZrO_2–CeO_2than in Ni/ZrO_2. The use of ZrO_2 has a beneficial effect particularly in the case of metals such as Pt, which is not good for promoting CO_2 dissociation (7). The high stability of the Pt/ZrO_2 catalysts has been connected to its ability to activate CO_2 (8). This feature is in turn assigned to the Pt atoms located at the Pt/ZrO_2 interface (9).

In the first part of this project, we investigated the behavior of Ni, Rh, and Ni–Rh formulations supported on La_2O_3. In that case, the most active and cleaner catalysts were those containing only Rh. In this case, in our search to develop catalysts suitable for membrane reactors, we have prepared and characterized (XRD, TPR, XPS, hydrogen chemisorption) several Ni–Rh supported on ZrO_2 solids. The nature and amount of the carbon deposits was further investigated through Raman spectroscopy, SEM, TGA, DSC, and TPH.

EXPERIMENTAL

Catalyst Preparation

Catalysts were prepared by conventional wet impregnation of ZrO_2 (Degussa) using $Ni(NO_3)_2 \cdot 6H_2O$ and $RhCl_3 \cdot 3H_2O$ as precursor compounds. The bimetallic solid was prepared by simultaneous impregnation. In all cases, the resulting suspension was then heated at 353 K to evaporate the water, and the solid material was dried in an oven at 383 K overnight. The resulting catalysts were calcined for 6 h at 823 K at a heating rate of 1.8 K/min. Both the Ni and Rh loadings were the same as those used when La_2O_3 was the support (10).

Catalyst Testing

The catalyst (50 or 300 mg) was loaded into a tubular quartz reactor (inner diameter, 5 mm) which was placed in an electric oven. A thermocouple in a quartz sleeve was placed on top of the catalyst bed. The catalysts were heated in He at 973 K and then reduced *in situ* in H_2 at the same temperature for 0.5 h. After reduction, the temperature was adjusted in flowing He to the reaction temperature (823–973 K), and the feed gas mixture (33% (v/v) CH_4, 33% CO_2, 34% He, $P = 1$ atm) was switched to the reactor.

[1] To whom correspondence should be addressed. E-mail: nfisico@fiqus.unl.edu.ar.

0021-9517/02 $35.00

The stability tests were carried out at $W/F = 2.67 \times 10^{-5}$ g h ml^{-1}, and conversion was measured at $W/F = 4.5 \times 10^{-6}$ g h ml^{-1}. The reaction products were analyzed in a TCD gas chromatograph (Shimadzu GC-8A) equipped with a Porapak column and a Molecular Sieve column.

Surface Area and XRD

For the determination of the surface area of calcined and used solids, a Quantachrome Sorptometer, Nova 1000 model, was employed. Prior to the BET measurements the samples were maintained at 473 K under vacuum of 10^{-3} Torr for 2 h.

The X-ray diffraction (XRD) patterns of the calcined and used solids were obtained with an XD-D1 Shimadzu instrument, using Cu $K\alpha$ radiation at 35 kV and 40 mA. The scan rate was 1° min^{-1} for values between $2\theta = 10$ and 80°.

X-Ray Photoelectron Spectroscopy

The XPS measurements were carried out using an ESCA750 Shimadzu electron spectrometer. Nonmonochromatic Al $K\alpha$ X-ray radiation was used. The anode was operated at 8 kV and 30 mA and the pressure in the analysis chamber was about 2×10^{-6} Pa.

The binding energies (B.E.) were referred to the C 1s signal (284.6 eV). Curve fitting was performed using a Levenberg–Marquardt NLLSCF routine. The background contribution was taken into account by assuming an integral-type background. The surface Rh/Zr and Ni/Zr atomic ratios were calculated using the areas under the Rh 3d, Ni $2p_{3/2}$, and Zr 3d peaks, the Scotfield photoionization cross sections, the mean free paths of the electrons, and the instrumental function, which was given by the ESCA manufacturer.

Metal Dispersion

The Rh dispersion of fresh catalysts, following the H_2 reduction at 973 K for 0.5 h, was determined by static equilibrium H_2 adsorption at room temperature in a conventional vacuum system. As a standard procedure, prior to adsorption, the catalysts (300 mg) were evacuated (10^{-5} Torr) at 573 K.

Temperature-Programmed Reduction

An Ohkura TP-20022S instrument equipped with a thermal conductivity detector (TCD) was used for the TPR experiments. The 100-mg samples were reduced in a 5% H_2–Ar stream, at a heating rate of 10 K min^{-1}.

Thermogravimetric Analysis

The amount of carbon on the used catalysts was determined by oxidizing the carbon in a Mettler Toledo TGA/SDTA 851. The used catalysts (usually 10 mg) were heated at 10 K min^{-1} to 1173 K in a flow of 90 ml min^{-1} air.

Thermal analysis experiments were carried out in a Mettler Toledo DSC 821^e in order to find out the exothermic or endothermic nature of the changes that take place during the calcination of the used solids.

Temperature-Programmed Hydrogenation

TPH experiments were carried out over used catalysts, and the solids (20 mg) were heated from 300 to 1073 K at 8 K min^{-1} under H_2 with a flow rate of 20 ml min^{-1}. The temperature was then kept constant for 1 h, and gases were analyzed by online mass spectrometry.

Laser Raman Spectroscopy

The Raman spectra were recorded with a TRS-600-SZ-P Jasco Laser Raman instrument, equipped with a CCD (charge coupled device) with the detector cooled to about 153 K using liquid N_2. The excitation source was the 514.5-nm line of a Spectra 9000 Photometrics Ar ion laser. The laser power was set at 30 mW.

RESULTS

Catalyst Characterization

Table 1 shows that the surface area of the ZrO_2 does not change after metal incorporation and further calcinations. The Rh dispersion data are also shown in Table 1. Note that the Ni solid after evacuation at 573 K does not adsorb H_2 at all.

Figure 1 shows the TPR traces for the Ni-Rh/ZrO_2 catalysts. The monometallic solids exhibit two reduction peaks. In the case of the Rh (0.2%) sample, the peaks' maxima are at 400 and 500 K, corresponding to easily reducible rhodium oxide. The TPR profile of our Ni/SiO_2 presents only one peak, at 629 K, indicating that there is no significant metal–support interaction. Xu *et al.* (11) reported TPR results for Ni-based catalysts supported on several oxides. The TPR of those high loading catalysts (~12 Ni wt%) showed one reduction peak (660–700 K) coincident with the reduction of unsupported nickel oxide. The Ni (2%) reduction profile

TABLE 1

Fresh Catalyst Features

Catalyst	S^a (m^2 g^{-1})	H/Rh^b	TPR^c H_2/metal
Rh (0.2%)	31.9	0.45	0.98
Ni (2%)	30.0	—^{d}	0.91
Ni (2%)–Rh (0.2%)	29.7	0.30	0.84

[a] BET surface area of calcined solids. The ZrO_2 support has 30 m^2 g^{-1}.
[b] Measured by H_2 chemisorption.
[c] Hydrogen consumption; 5% H_2 in Ar, 10 K min^{-1}.
[d] This solid does not adsorb H_2.

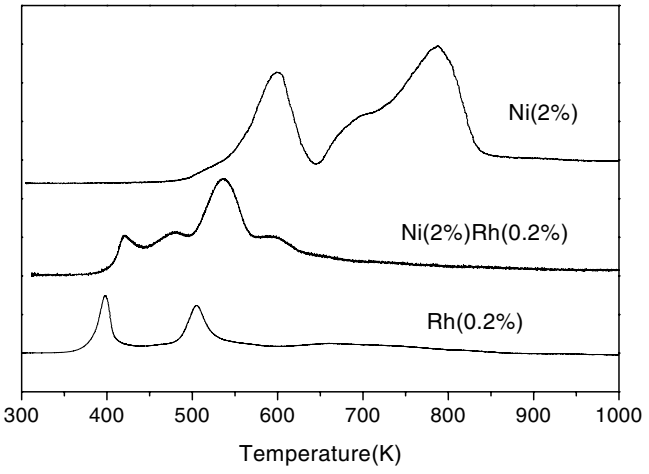

FIG. 1. TPR profiles of calcined Ni–Rh catalysts (5% H_2 in Ar, 30 ml min^{-1}, 10 K min^{-1}).

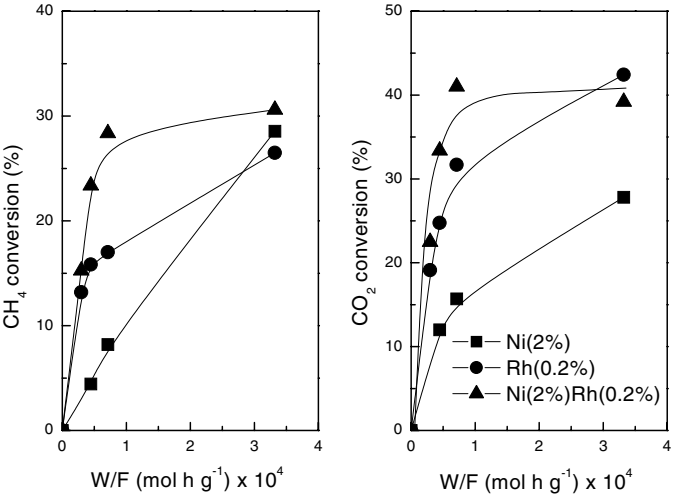

FIG. 2. Catalytic behavior of Ni–Rh solids at 823 K, 33% (v/v) CH_4, 33% CO_2, 34% He, $P = 1$ atm.

of our solid reveals two peaks, at 618 and 760 K. The low-temperature peak may be assigned to well-dispersed nickel oxide in the support while the highest temperature peak is symptomatic of a strong metal support interaction. One possibility is the formation of a mixed oxide. However, the Raman spectra and XRD patterns of Ni/ZrO_2 catalysts show no presence of Ni phases.

The TPR profile of the bimetallic solid is more complex, probably due to additional Ni-Rh interaction. The total H_2 consumption is reported in Table 1.

Stability and Reaction Rates of Ni–Rh/ZrO_2 Catalysts

In order to compare the catalytic performance of the solids at low temperature, initial reaction rates of methane and carbon dioxide were calculated (Table 2) from CH_4 and CO_2conversions vs W/F curves (Fig. 2) determined at 823 K. The bimetallic catalyst is the most active and the Ni (2%) had the worst performance. The turnover frequency values (H/Rh from Table 1 were used to calculate TOFs) of the catalysts are also shown in Table 2.

As clearly shown in Fig. 3, over a testing period of 100 h, there is practically no loss of activity over the Rh (0.2%) catalyst, while the other two formulations do deactivate. Note, however, that both TGA and TPH measurements show that no carbon deposition has occurred on the catalysts kept on stream up to 100 h at 823 K.

XPS Data of Fresh and Used Ni–Rh Catalysts

The peak positions and FWHM of the Rh $3d_{5/2}$, Ni $2p_{3/2}$, and Zr $3d_{5/2}$ are summarized in Table 3. In the monometallic Rh solid, the Rh $3d_{5/2}$ binding energy did not change after 48 h on stream and only a slight peak broadening was observed.

Surface atomic ratios for the fresh and used samples are given in Table 4. In the case of the fresh Rh (0.2%) solid, the Rh/Zr atomic ratio is 0.012. This ratio remains constant after reaction at temperatures between 823 and 973 K. For the bimetallic sample, the high B.E. for Rh $3d_{5/2}$ (308.9 eV) and Ni $2p_{3/2}$ (856.3 eV) indicate the presence of oxidized surface species (12–15). In this sample, the Rh/Zr and Ni/Zr are 0.022 and 0.08, respectively. However, after 48 h on stream under the same reaction conditions, no signal from Rh and Ni was detected. A large signal from carbon (283.2 eV) was

TABLE 2

Catalytic Behavior of ZrO_2-Supported Catalysts

Catalyst[a]	X_{CH_4}[b] (76.6)	X_{CO_2}[b] (84.9)	R_{CH_4}[c] (mol g^{-1} h^{-1})	R_{CO_2}[c] (mol g^{-1} h^{-1})	TOF_{CH_4} (s^{-1})	TOF_{CO_2} (s^{-1})
Rh (0.2%)	83.1	87.3	0.32	0.50	11.0	16.5
Ni (2%)	65.9	67.9	0.09	0.24	—	—
Ni (2%)–Rh (0.2%)	74.7	78.9	0.47	0.67	21.5	31.3

[a] Solids were reduced *in situ* at 973 K before reaction. Weight percent of transition metals is in parentheses.

[b] Initial percentage conversions measured at reaction temperature = 973 K, $W/F = 1.05 \times 10^{-5}$ g h ml^{-1}; total reaction time 48 h. Equilibrium values, in parentheses, were calculated using a $CH_4 + CO_2$ reaction and the reverse WGSR.

[c] Initial reaction rates measured at 823 K (conversion values, <10%).

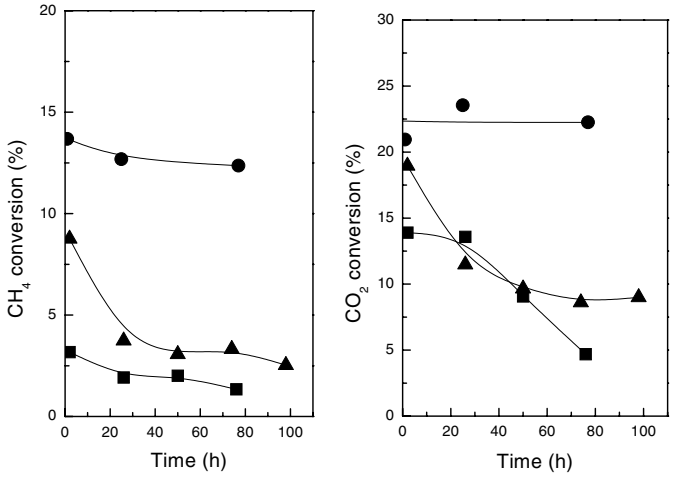

FIG. 3. Stability test carried out at $W/F = 2.67 \times 10^{-5}$ g h ml^{-1}, $T = 823$ K, 33% (v/v) CH_4, 33% CO_2, 34% He, $P = 1$ atm; conversion measurements at $W/F = 4.5 \times 10^{-6}$ g h ml^{-1}.

observed, assigned to residues formed during the reaction. Similar results were obtained for Ni (2%) supported on ZrO_2. The atomic C/Zr ratio was lower for this solid compared to the bimetallic one. The C 1s spectrum of the used Rh (0.2%) sample showed a very weak carbon deposit peak.

Long-term stability tests caused the Rh/Zr and Ni/Zr atomic ratios to decrease to 0.013 and 0.053 for the Ni (2%)–Rh (0.2%) sample. No carbon peak at 283.2 eV was detected. These results are in agreement with the data obtained from TGA and Raman spectroscopy (vide infra). For this solid, a significant broadening was shown in the Rh $3d_{5/2}$ peak. This could be due to a partial reoxidation of the sample after exposure to ambient conditions. This explanation is supported by the presence of a low binding energy peak in the Ni $2p_{3/2}$ spectrum.

Carbon Deposits after Catalytic Tests in Equilibrium Conditions

The equilibrium conversion for the CO_2 reforming and the water–gas shift reaction were closely approached in the whole temperature range investigated when appropriate space velocities were used over Rh catalysts, as shown in Table 2. Table 5 shows the surface area of used catalysts after being on stream for 48 h at temperatures up to 973 K. The space velocities were low in order to achieve near-equilibrium conversion all along these runs. Note that neither monometallic catalyst shows a change in surface area (see also Table 1) beyond the experimental error. However, a large increase in surface area is observed in the bimetallic solid.

Figure 4 shows the diffractograms of the used catalysts and the ZrO_2 support. In the latter, both the tetragonal ($2\theta = 30.1^\circ$) and the monoclinic phases coexist. In the used catalysts, the main reflection of the tetragonal phase sharply decreases in intensity, as expected, since this structure is less stable at higher temperatures. Note that the Ni-containing solids show a wide reflection at 26 which can be assigned to graphitic carbon (16). This peak does not appear in the Rh (0.2%) solid.

TGA was used to quantify the amount of carbon deposits on the three catalysts. The TGA profiles are shown in Fig. 5, and the amount of carbon burnt is shown in Table 5. The Rh (0.2%) catalyst only shows a small mass loss at 587 K. Note that this peak also appears in the bimetallic solid. The Ni-containing formulations exhibit similar TGA profiles (Fig. 5). The only difference is the lower temperatures at which the carbon is burnt in the bimetallic catalyst. This lower temperature may be due to either a catalytic effect of Rh during carbon burning or different reactivities of the carbon residues. The DSC data (not shown) confirm that all the mass changes detected in the TGA experiments are exothermic processes that are likely to be the burning of the carbonaceous residues.

Another way to study the reactivity of residues is to use TPH (Fig. 6). Three peaks of methane ($m/e = 16$) were detected on the Ni (2%) catalyst, at 573, 800, and 990 K. These may be assigned to either different types of carbon deposits or deposits formed on different locations (support, metal, or metal/support interface). The used bimetallic catalyst only exhibits two peaks while the Rh (0.2%) only shows a

TABLE 3

Binding Energies of Ni–Rh Catalysts[a]

Catalyst	Calcined			Used (48 h)			Used (100h)		
	Zr $3d_{5/2}$	Rh $3d_{5/2}$	Ni $2p_{3/2}$	Zr $3d_{5/2}$	Rh $3d_{5/2}$	Ni $2p_{3/2}$	Zr $3d_{5/2}$	Rh $3d_{5/2}$	Ni $2p_{3/2}$
Rh (0.2%)	182.2 (1.7)	308.2 (2.4)	—	182.2 (1.9)	308.4 (2.9)	—	—	—	—
Ni (2%)–Rh (0.2%)	182.2 (1.7)	308.9 (2.8)	856.3 (3.0)	182.2	nd[b]	nd	182.2 (2.0)	308.0 (3.6)	856.2 (2.7) 853.9 (3.7)
Ni (2%)	182.2	—	856.0 (3.2)	182.2	—	nd	182.2 (2.0)	—	nd

[a] Contamination carbon was taken as reference at 284.6 eV. FWHM values are shown in parentheses.
[b] nd, not detected.

TABLE 4

Surface Atomic Ratios of Ni–Rh Catalysts

Catalyst	Calcined			Used (48 h)[a]				Used (100h)[b]			
	$(Rh/Zr)_s$	$(Ni/Zr)_s$	$(O/Zr)_s$	$(C/Zr)_s$[c]	$(Rh/Zr)_s$	$(Ni/Zr)_s$	$(O/Zr)_s$	$(C/Zr)_s$	$(Rh/Zr)_s$	$(Ni/Zr)_s$	$(O/Zr)_s$
Rh (0.2%)	0.012	—	2.6	0.3	0.017	—	2.2	nm[e]	nm	nm	nm
Ni (2%)–Rh (0.2%)	0.022	0.08	2.4	12.0	nd[d]	nd	3.2	0	0.013	0.053	2.6
Ni (2%)	—	0.059	2.3	9.1	—	nd	4.0	—	—	—	—

[a] Reaction temperature, 823–973 K.
[b] Reaction temperature, 823 K.
[c] Carbon at 283.2 eV. Contamination carbon was taken as reference at 284.6 eV. No carbon at 283.2 eV was observed on the calcined samples.
[d] nd, not detected.
[e] nm, not measured.

small methane peak. To check the extent of hydrogenation of the residues, a second TGA was performed in air after the TPH experiment. In the TGA profile, two peaks are observable at temperatures similar to the former ones. By comparing the mg C/g catalyst ratios, it is concluded that the residues most difficult to oxidize were not significantly reduced. The second most difficult to oxidize deposits were roughly 50% consumed during the TPH experiments. The easiest to oxidize residue was completely wiped out by the reducing stream.

All the Raman spectra (Fig. 7) of the used catalysts invariably showed two peaks, at 1350 and 1580 cm^{-1}, which are assigned to graphitic carbon (17). The signal intensity in the Rh (0.2%) catalyst was very weak compared to the other two solids. Furthermore, in the Ni-containing solids no signals from ZrO_2 were detected, even though several pellet areas were scanned. This is consistent with the presence of significant amounts of carbonaceous deposits which completely cover the catalyst particles.

The SEM micrographs clearly show the presence or carbon filaments on top of both the Ni (2%) and Ni (2%)–Rh (0.2%) catalysts (Fig. 8). In the latter case, the carbon deposit completely covers the catalyst particles. On the other hand, the SEM micrograph of Rh (0.2%) does not reveal the presence of carbonaceous residues which were, however, detected by the other techniques (TGA, TPH, and LRS), although in tiny amounts (Table 5).

TABLE 5

Amount of Carbonaceous Residues Formed on Used Catalysts

Catalyst	S^a ($m^2\ g^{-1}$)	TGA[b]		TGA[c]	
		$mg_{carbon}/g_{cat.}$	T_p[d] (K)	$mg_{carbon}/g_{cat.}$	T_p[d] (K)
Rh (0.2%)	29.4	10	587	—	—
Ni (2%)	32.4	245	810	119	805
		95	940	82	963
Ni (2%)–Rh (0.2%)	45.1	6	585	—	—
		290	770	134	773
		135	900	112	929

[a] BET surface area of used catalysts.
[b] Time on stream, 48 h; reaction temperature, between 823 and 973 K; $W/F = 1.07 \times 10^{-5}$ g h ml^{-1}.
[c] Same as above, after TPH experiments.
[d] Peak temperature.

DISCUSSION

This study originated in the need to find stable catalysts with the lowest carbon deposition level able to operate at 823–873 K, for use in membrane reactors. For obvious

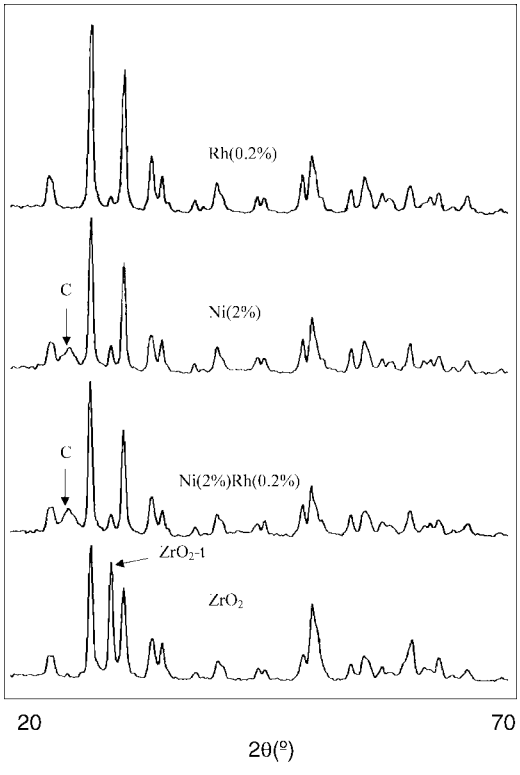

FIG. 4. DRX patterns of used Ni–Rh catalysts after 48 h on stream (see Table 5) and support. Scan rate: 1 min^{-1}.

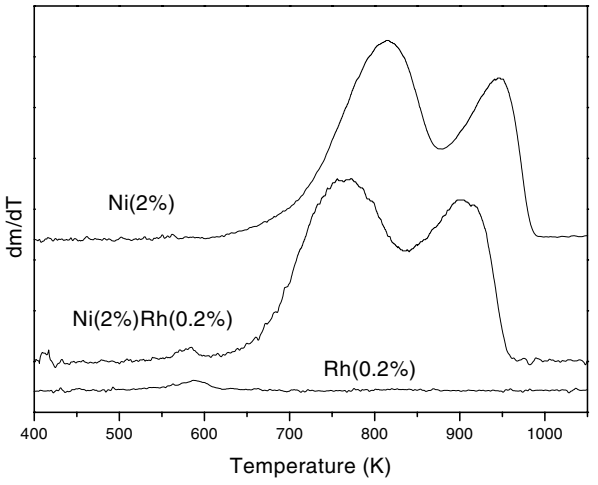

FIG. 5. TGA profiles of used solids. Time on stream 48 h; temperature range, 823–973 K; $W/F = 1.07 \times 10^{-5}$ g h ml^{-1}.

reasons most of the published studies to date have been carried out at $T > 873$ K. In addition, scarce data are available at any temperature for Rh on ZrO_2 systems. The data presented and the following discussion will be useful for visualizing the similarities and differences observed between low- and high-temperature operation.

Carbon Deposits

Carbon deposition is a fundamental problem in the carbon dioxide reforming reaction. The origin of the inactive carbon can be methane decomposition and CO disproportion (4). The carbon formed is frequently in the form of filamentous whiskers (18), but the most deactivating one is the encapsulating type (19). In Rh catalysts supported over Y-stabilized ZrO_2 a very low deactivation rate was observed (20), while in the Ce-doped Ni catalysts over ZrO_2 (6) the coke formation did not affect the catalytic activity.

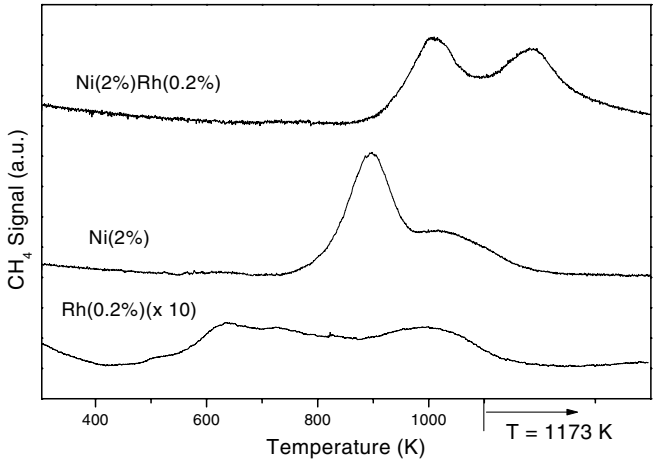

FIG. 6. TPH profiles of used solids. Time on stream 48 h; 823–973 K; $W/F = 1.07 \times 10^{-5}$ g h ml^{-1}.

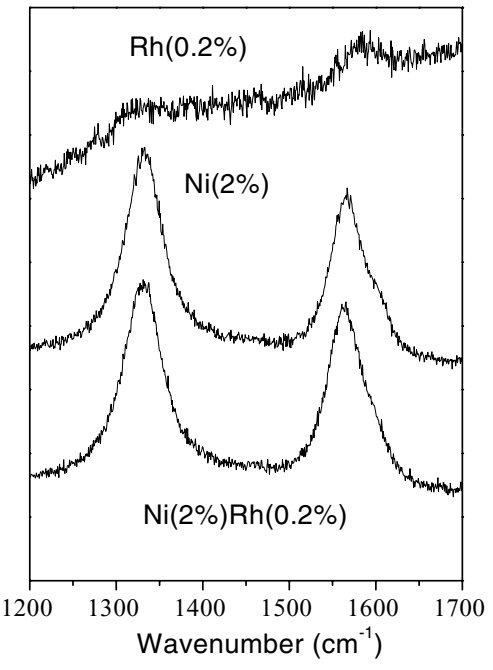

FIG. 7. Raman spectra of Ni–Rh catalysts used 48 h in reforming reaction. Temperature range, 823–943 K; $W/F = 1.07 \times 10^{-5}$ g h ml^{-1}.

Carbon deposits invariably appear on our catalysts assayed near equilibrium conditions at 823–973 K (Table 5). Large amounts of carbonaceous material are formed on both Ni (2%) and Ni (2%)–Rh (0.2%) catalysts. The SEM micrographs show the abundant formation of filaments (Fig. 8). Both DRX and LRS indicate the presence of graphitic carbon (Figs. 4 and 7). The appearance of peaks in both the TGA (Fig. 5) and TPH (Fig. 6) profiles is symptomatic of either the presence of two carbon species with different reactivity or carbon deposited on different surface sites, or both. In $Pt/Ce_xZr_{1-x}O_2$, Noronha *et al.* (7) found that the different peaks in the TPO profile (similar to ours) are not due to different forms of carbon but rather to different locations on the catalyst surface. The low-temperature peak was assigned to carbon near the metal particles, and the high-temperature peak to carbon deposited on the support.

In agreement with what has been reported by Nagaoka *et al.* (8) the TGA experiments, performed after the TPH, show that the carbon which oxidizes at higher temperature cannot be removed by reaction with hydrogen up to 1173 K (Table 5). The carbonaceous deposits formed in our Ni-Rh catalysts could be deposited on the metals and on the support. The deposits on the support would require temperatures over 1173 K to react with H_2.

The monometallic Rh catalyst exhibits a very-low-carbon deposition. For this solid, the XPS surface C/Rh ratio was equal to 15 (Table 4). No changes were observed in the surface Rh/Zr ratio after 48 h on stream, suggesting that

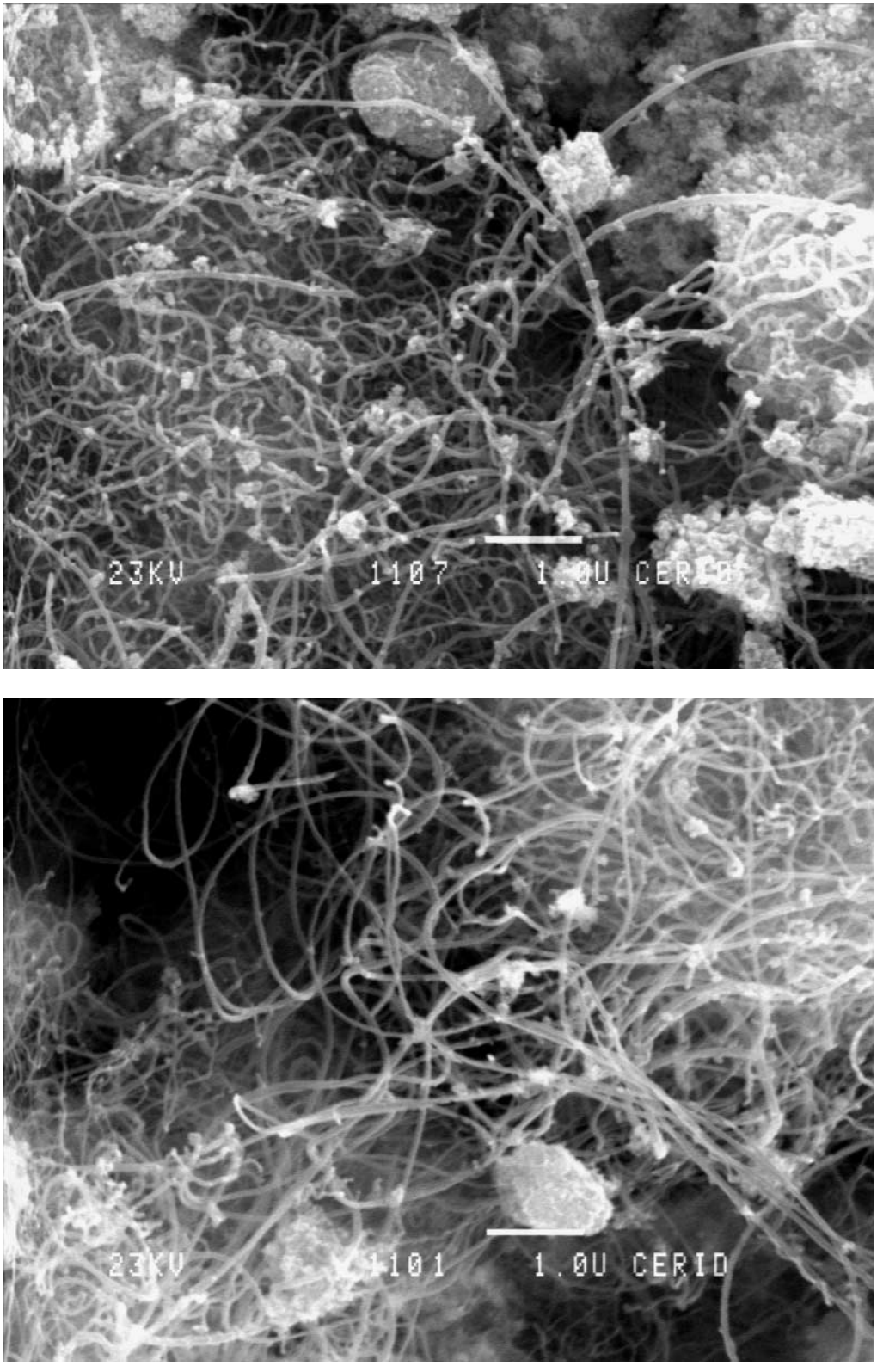

FIG. 8. SEM micrographs of Ni (2%) and Ni (2%)–Rh (0.2%) after 48 h on stream at $W/F = 1.07 \times 10^{-5}$ g h ml^{-1}; temperature range, 823–973 K.

no sintering occurred due to the high reaction temperature.

Stability and Reaction Rates of Ni–Rh/ZrO_2 Catalysts at Low Temperature

Bitter *et al.* (9) have suggested that the oxide supports which are good oxygen donors, such as ZrO_2, yield excellent catalysts for the dry reforming of methane. When Rh is the active metal used in this reaction, most of the published work concerns the effect of several supports upon the catalytic performance. The most common supports are ZrO_2, TiO_2, Al_2O_3, SiO_2, and MgO (20).

Zhang *et al.* (20), comparing the initial activity of Rh catalysts and the acidity of the carriers, stated that a correlation between TOF and surface acidity seems to exist. It appears that the acidic nature of the carrier may promote methane dissociation on the sites at the periphery of metal crystallites (metal–support interface). They found that the initial intrinsic activity and rate of deactivation of Rh decrease with increasing metal particle size. They maintained that the higher the dispersion, the higher the metal–support interfacial area, which results in more intense metal–support interactions.

Table 6 shows the TOF of our Rh/ZrO_2 and Rh/La_2O_3 (10) catalysts together with data reported in the literature for the same systems. The data show that both the specific activity and the activity per mole of Rh of our Rh/ZrO_2 catalyst is the highest of them all. Note that this catalyst (Fig. 3) and the Rh/La_2O_3 (10) are stable after 100 h on stream at 823 K.

In the case of the Ni monometallic solid, low activity and a high deactivation rate were observed (Table 2 and Fig. 3). Adding Rh to the Ni solid produced an active catalyst but the deactivation rate was increased. However, no carbon formation was observed in these catalysts.

Since there are scarce data concerning the nature of the Rh/ZrO_2 interaction for dry reforming, in what follows we will make frequent reference to the related system of Pt/ZrO_2. For the latter system, a number of studies (3, 4, 7) have been published. They are mainly aimed at understanding the nature of the activity and stability behavior of these solids. Ross and co-workers (21), using a TAP reactor (temporal analysis of products), observed that on Pt/ZrO_2 both methane and carbon dioxide dissociate independently of one another. The dissociation of carbon dioxide acts as an oxygen supplier, while the decomposition products of methane scavenge the oxygen from the catalyst. According to this mechanism, CH_4 decomposition would take place on the metal (22), resulting in the production of H_2 and the formation of carbonaceous deposits. The role of the support would be to adsorb CO_2 and allow the dissociation at the metal–support interface.

In the Pt/ZrO_2 system, Stagg *et al.* (23) found that when the rate of CH_4 decomposition is initially greater than the rate of CO_2 dissociation, carbon deposition occurs and is responsible for the deactivation of the catalyst. The stability of the catalysts depends on the balance between the two paths.

They proposed a cleansing mechanism where the carbon is removed from the metal particles. The dissociation of CO_2 leads to the formation of CO and adsorbed O, which can then combine with carbon on the metal to form additional CO. Another possibility is that the oxygen that reacts with the carbon comes from the support.

Using pulse experiments with ^{13}C-labeled CH_4, they found that Pt is needed to catalyze the dissociation of CO_2. Then, the dissociation can take place near the metal–support interface or can occur on oxygen vacancies generated during the previous reduction of the support. Our monometallic Rh catalyst supported on ZrO_2 is very stable and does not present carbon deposition. Considering that CO_2 dissociates on Rh surface (24), a similar cleansing reaction mechanism could be proposed for our stable Rh/ZrO_2 solid. Besides, the XPS Rh/Zr ratio did not change after 48 h on stream (Table 4), suggesting that Rh dispersion remains unchanged.

TABLE 6

Reaction Rates, TOF Values, and Deactivation of Rh Catalysts

Catalyst	*D* (%)	Temp. (K)	R_{CH_4}[a] mol h^{-1} g^{-1}	R_{CH_4}[a] mol h^{-1} g^{-1} Rh	R_{CO_2}[a] mol h^{-1} g^{-1}	R_{CO_2}[a] mol h^{-1} g^{-1} Rh	TOF (s^{-1}) CH_4	TOF (s^{-1}) CO_2	θ_{react}[b] (h)	Deac[c] (%)	Ref.
Rh (0.2%)/ZrO_2	45[d]	823	0.32	160	0.50	250	11.0	16.5	100	0	This work
Rh (0.2%)/La_2O_3	64[d]	823	0.20	100	0.42	210	4.4	9.1	100	0	10
Rh (0.6%)/La_2O_3	14[d]	823	0.26	43	0.51	85	13.8	16.7	100	0	10
Rh (0.5%)/ZrO_2	90[d]	875	—	—	0.34	68	—	2.2	70	0	6
Rh (1.0%)/ZrO_2	16[e]	873	0.05	5	—	—	0.9	—	48	0	11

[a] Initial reaction rates, calculated from data given by the authors.
[b] Time on stream.
[c] Deactivation.
[d] Dispersion measured by H_2 chemisorption.
[e] Dispersion measured by CO chemisorption.

Van Keule *et al.* (21) maintained that the oxygen pool used for the reactions described is present in the vicinity of the Pt crystallites. They emphasized that ZrO_2 can be partially reduced, leading to the formation of Pt–Zr surface alloys. This surface alloy helps to maintain a high Pt dispersion. Since Rh–Zr alloys do exist (25), the same beneficial effect could be present in the Rh/ZrO_2 catalyst.

ZrO_2 is well-known for its ability to interact strongly with the metal component and, therefore, to stabilize the metallic Rh cluster (15). In the Ni–Rh bimetallic solid the TPR profile (Fig. 1) suggests the presence of a strong interaction between the metals, and the low-binding-energy Ni $2p_{3/2}$ peak (Table 3) indicates the formation of stable reduced species in the catalysts after 100 h on stream. These species did not reoxidize after being exposed to air. The results of both techniques are consistent with the formation of a Ni–Rh surface alloy (12). As no carbon deposition has occurred on this solid when kept on stream for up to 100 h at 823 K, one explanation for the deactivation observed in the Ni–Rh solid could be that the presence of Ni decreases the interaction between the Rh and the support at the particle–support interface. A similar effect was previously reported by Stagg *et al.* (23) in $Pt–Sn/ZrO_2$ catalysts.

Bradford and Vannice (26) have reported that the presence of a TiO_x overlayer on the Pt surface reduces the number of large ensembles of Pt atoms and geometrically inhibits CO dissociation and CH_4 decomposition. This is consistent with Zhang *et al.* (20). They attributed the high activity and stability of Ni/La_2O_3 catalysts to LaO_x species on the Ni surface.

Considering available literature data, Bradford and Vannice (26) assigned the higher stability and coking resistance of Pt/ZrO_2 to strong $Pt–Zr^{n+}$ interactions which block active sites for carbon deposition and results in the formation of ZrO_x species on the Pt surface. Roberts and Gorte (27) indicated that ZrO_2 influences the Pt surface via a strong Zr^{n+}–Pt interaction, altering particle morphology and lowering the CO desorption barrier.

Comparing the XANES results with TPR, Bitter *et al.* (3) assigned the high-reduction-temperature peak at 632 K (from TPR) to the partial reduction of ZrO_2. They speculated that hydrogen is activated on Pt and partially reduces ZrO_2 in its direct vicinity. In our TPR profiles for the Ni–Rh/ZrO_2 catalyst, the reduction temperature peak at 632 K was not observed; therefore, no partial reduction of the support seems to occur.

Three factors (20) may influence the deactivation of these catalysts, namely the deposition of carbonaceous residues, metal particle sintering, and blockage of Rh surface sites by species originated in the support. The absence of carbon deposition at 823 K eliminates the first factor. Metal sintering seems to be minimized due to the metal–support interaction evidenced by TPR and XPS.

When the reaction is conducted at high temperature, carbon deposition occurs on the bimetallic solids. This could be the result of an interplay between CH_4 dissociation and CO_2 decomposition. The former is favored by higher temperatures and perhaps the CO_2 decomposition does not proceed fast enough to burn the carbonaceous residues left on the surface. An alternative view is that the ZrO_2 support could provide lattice oxygen to clean the surface at a slow rate at high temperature. In any case, the experimental data indicate that CO disproportionation is not responsible for carbon formation on the Ni–Rh catalysts.

Previously, we used $Ni–Rh/La_2O_3$ catalysts for dry reforming of methane (10). We found that the formation of carbonaceous residues does not affect the catalytic activity of these formulations. We have also detected strong metal–support interaction associated with the high specific activity and stability of the $Ni–Rh/La_2O_3$ formulations. Table 6, which includes the activity data for the La_2O_3 catalysts, shows that Rh/ZrO_2 is the most active catalyst, as stable as those supported on La_2O_3 (100 h on stream).

CONCLUSIONS

Rh (0.2%)/ZrO_2 is the most active, stable catalyst for CO_2 reforming at 823 K. Only small amounts of carbonaceous residues (TGA, XPS) were formed after 48 h on stream at temperatures up to 973 K. No residues were detected at 823 K after 100 h on stream. Therefore, this catalyst is suitable for use in membrane reactors. Besides, compared with published data of Rh supported on different ceramic oxides, the Rh (0.2%)/ZrO_2 solid results in the most active formulation on a per-gram-of-rhodium basis. Our data suggest that the origin of this remarkable performance is a strong interaction between rhodium and ZrO_2.

Carbon deposits formed on Ni-containing catalysts used at high temperature are mostly graphitic filaments, probably formed on different surface sites, exhibiting different reactivities.

In the bimetallic formulation, the formation of Ni–Rh alloys is likely to be responsible for the deactivation of this solid at 823 K when carbonaceous deposits are negligible. The formation of Ni–Rh alloys would impair the strong Rh/ZrO_2 interaction.

ACKNOWLEDGMENTS

The authors acknowledge the financial support received from UNL, CONICET, and ANPCyT. Thanks are given to the Japan International Cooperation Agency (JICA) for the donation of the major instruments, to Elsa Grimaldi for editing the English, to Fabricio Charles and John Munera for their technical assistance, and to Prof. María Alicia Ulla for her helpful discussions.

REFERENCES

1. Kikuchi, E., Wemoto, Y., Kejiwara, M., Vemiya, S., and Kojima, T., *Catal. Today* **56**, 75 (2000).
2. Wang, H., and Ruckenstein, E., *Appl. Catal. A* **204**, 143 (2000).
3. Bitter, J., Seshan, K., and Lercher, J., *J. Catal.* **176**, 93 (1998).

4. Bradford, M., and Vannice, M., *Catal. Rev.–Sci. Eng.* **41**(1), 1 (1999).
5. Wang, S., and Lu, G., *Appl. Catal. B* **16**, 269 (1998).
6. Montoya, A., Romero, E., Guimon, C., and Monzón, A., *Catal. Today* **63**, 71 (2000).
7. Noronha, F., Fendley, E., Soares, R., Alvarez, W., and Resasco, D., *Chem. Eng. J.* **82**, 21 (2001).
8. Nagaoka, K., Seshan, K., Lercher, J., and Aika, K., *Catal. Lett.* **70**, 109 (2000).
9. Bitter, J. H., Seshan, K., and Lercher, J. A., *Top. Catal.* **10**, 295 (2000).
10. Irusta, S., Cornaglia, L. M., and Lombardo, E. A., *J. Catal.*, in press.
11. Xu, Z., Li, Y., Zhang, J., Chang, L., Zhou, R., and Duan, Z., *Appl. Catal. A* **210**, 45 (2001).
12. Lei, H., Song, Z., Tan, D., Bao, X., Mu, X., Zong, B., and Min, E., *Appl. Catal. A* **214**, 69 (2001).
13. McIntyre, N., and Cook, H., *Anal. Chem.* **47**(13), 2208 (1975).
14. Sigl, M., Bradford, M., Knözinger, H., and Vannice, A., *Top. Catal.* **8**, 211 (1999).
15. Pechi, G., Reyes, P., Gómez, R., López, T., and Fierro, J., *Appl. Catal. B* **17**, L7 (1998).
16. Wang, S., *Energy Fuels* **12**, 248 (1998).
17. Tuinstra, F., and Koenig, J., *J. Chem. Phys.* **53**, 1126 (1970).
18. Takenaka, S., Ogihara, H., Yamanaka, I., and Otsuka, K., *Appl. Catal. A* **217**, 101 (2001).
19. Kroll, V., Swaan, H., and Mirodotos, C., *J. Catal.* **161**, 409 (1996).
20. Zhang, Z., Tsipouriari, V., Etstethiou, A., and Verykios, X., *J. Catal.* **158**, 51 (1996).
21. Van Keule, A., Seshan, K., Hoebink, J., and Ross, J., *J. Catal.* **166**, 306 (1997).
22. Bitter, J., Seshan, K., and Lercher, J., *J. Catal.* **171**, 279 (1997).
23. Stagg, W., Romeo, E., Padro, C., and Resasco, A., *J. Catal.* **178**, 137 (1998).
24. Van Tol, M., and Gielbert, A., *Appl. Surf. Sci.* **67**, 166 (1993).
25. Moffett, W., "The Handbook of Binary Phase Diagrams," Vol. 4. General Electric Co., 1978.
26. Bradford, M., and Vannice, M. A., *J. Catal.* **173**, 157 (1998).
27. Roberts, S., and Gorte, R., *J. Phys. Chem.* **95**, 5600 (1991).